Contribution from the Dipartimento di Scienze Chimiche, University of Catania, 95125 Catania, Italy, Department of Chemistry and Materials Research Center, Northwestern University, Evanston, Illinois 60208, and Istituto di Chimica, University of Basilicata, 85100 Potenza, Italy

Electronic Structure of Tetracoordinate Transition-Metal Complexes. 5. Comparative Theoretical ab Initio/Hartree-Fock-Slater and Ultraviolet-Photoelectron Spectroscopic Studies of Building Blocks for Low-Dimensional Conductors. Dibenzo[*b*,*i*][1,4,8,11]tetraazacyclotetradecine Complexes of Nickel(II) and Palladium(II)†

Maurizio Casarin,[1a] Enrico Ciliberto,[1b] Santo Di Bella,[1b] Antonino Gulino,[1b] Ignazio Fragalà,*[,1b] and Tobin J. Marks*[,1c]

Received March 21, 1991

The electronic structure of the Ni and Pd complexes of the title ligand have been studied by an integrated experimental He I/He II photoelectron spectroscopic as well as theoretical ab initio pseudopotential and first-principles local exchange DV-Xα approach. Theoretical calculations have provided a complete assignment of photoelectron spectra as well as useful information on the peculiarities of the valence electronic system that, in turn, is of relevance in understanding the properties of low-dimensional, partially oxidized, $[M(TAA)^{\rho+}]_n$ systems. Furthermore, similarities and differences between the present complexes and partially oxidized metallophthalocyanines are discussed in terms of the nature of the HOMO and of twisting motion effects upon the valence bandwidths. The present results argue that the charge transport in tetraazaannulene molecular conductors occurs via bands that are predominantly ligand π-electron in character, and that twisting motions (librations) scarcely affect the resistivity.

Introduction

Recently, much attention has been devoted to the preparation and characterization of low-dimensional materials having unusual, frequently "metal-like" charge-transport properties.[2] Among them, a particularly attractive class is based on metal complexes of the dibenzo[*b*,*i*][1,4,8,11]tetraazacyclotetradecine (TAA) ligand[3] (Chart I). These molecular species consist of conjugated macrocycles having an MN_4 core (M = metal). Oxidative interactions of the metal-free 5,14-dihydrodibenzo[*b*,*i*][1,4,8,11]-tetraazacyclotetradecine (H_2TAA) and of some of its metal complexes M(TAA) (M = Ni, Pd, Pt, Co, Cu) with various oxidants (halogens, 7,7,8,8-tetracyanoquinodimethane) results in the formation of low-dimensional conducting solids having a nonintegral formal oxidation state.[4] Although different in molecular structure and symmetry, TAA complexes exhibit distinct similarities to metallophthalocyanines and -porphyrins in regard to electrochemical properties,[5] optical spectra,[3c] and metal-like electrical conductivities when partially oxidized.[4d,e,6,7]

It has been shown that integrated electronic structure studies of metal complex building blocks of low-dimensional conductors using He I/He II photoelectron spectroscopy (PES) measurements combined with high-quality ab initio and first-principles Hartree-Fock-Slater theoretical calculations are ideally suited[8,9] to answer presently unresolved questions on intermolecular interactions among metal-based and/or ligand-based orbitals of the molecular subunits in the infinite stacks. Hence, such studies are of major relevance in fully understanding solid-state chemical and physical properties. Furthermore, this information will be of importance in understanding similarities and differences between the present complexes and other conductive metallomacrocycle-based materials.

For these reasons, as a part of on-going studies on conducting materials based on planar d^8 metal complexes,[9,10] we report in this paper on the electronic structure of the H_2TAA molecule and of the related Ni(TAA), Pd(TAA), and Pd(TMTAA) (palladium 2,3,11,12-tetramethyldibenzo[*b*,*i*][1,4,8,11]tetraazacyclotetradecine) complexes (Chart I). The implications on the charge-transport properties of these complexes are discussed as well.

Experimental Section

The compounds of interest were prepared according to literature methods,[3] and were purified by sublimation in vacuo.

PE spectra were recorded with the aid of a photoelectron spectrometer interfaced to an IBM PC AT computer as described elsewhere.[9] The spectra were recorded at temperatures of 250 °C for H_2TAA and Ni(TAA) and 350 °C for Pd(TMTAA) and Pd(TAA). The energy scale

† Abstracted in part from the Ph.D. thesis of S. Di Bella, University of Catania, 1986.

(1) (a) University of Basilicata. (b) University of Catania. (c) Northwestern University.
(2) (a) Jérome, D., Caron, L. G., Eds. *Low-Dimensional Conductors and Superconductors*; Plenum: New York, 1987. (b) Rouxel, J., Ed. *Crystal Chemistry and Properties of Materials with Quasi-One-Dimensional Structures*; Reidel: Dordrecht, 1986. (c) Monceau, P., Ed. *Electronic Properties of Inorganic Quasi-One-Dimensional Compounds*; Reidel: Dordrecht, 1985. (d) Miller, J. S., Ed. *Extended Linear Chain Compounds*; Plenum: New York, 1982; Vols. 1, 2; 1983; Vol. 3. (e) Devreese, J. T., Evrard, R. P., Van Doren, V. E., Eds. *Highly Conducting One-Dimensional Solids*; Plenum: New York, 1979. (f) Miller, J. S.; Epstein, A. J. *Prog. Inorg. Chem.* **1976**, *20*, 1.
(3) (a) Cotton, F. A.; Czuchajowska, J.; Feng, X. *Inorg. Chem.* **1990**, *29*, 4329. (b) Cutler, A. R.; Alleyne, C. S.; Dolphin, D. *Inorg. Chem.* **1985**, *24*, 2276, 2281. (c) Sakata, K.; Hashimoto, M.; Tagami, N.; Murakami, Y. *Bull. Chem. Soc. Jpn.* **1980**, *53*, 2262. (d) Tsutsui, M.; Bobsein, R. L.; Cash, G.; Pettersen, R. *Inorg. Chem.* **1979**, *18*, 758. (e) Weiss, M. C.; Gordon, G.; Goedken, V. L. *Inorg. Chem.* **1977**, *16*, 305. (f) Goedken, V. L.; Pluth, J. J.; Peng, S. M.; Bursten, B. *J. Am. Chem. Soc.* **1976**, *98*, 8014. (g) Neves, D. R.; Dabrowiak, J. C. *Inorg. Chem.* **1976**, *15*, 129. (h) Lin, L.-S. Ph.D. Thesis, Northwestern University, Evanston, IL, 1980.
(4) (a) Spellane, P. J.; Interrante, L. V.; Kullnig, R. K.; Tham, F. S. *Inorg. Chem.* **1989**, *28*, 1587. (b) Hunziker, M.; Rihs, G. *Inorg. Chim. Acta* **1985**, *102*, 39. (c) Marks, T. J.; Kalina, D. W. In *Extended Linear Chain Compounds*; Miller, J. S., Ed.; Plenum: New York, 1982; Vol. 1, p 197. (d) Hunziker, M.; Hilti, B.; Rihs, G. *Helv. Chim. Acta* **1981**, *64*, 82. (e) Hunziker, M.; Loeliger, H.; Rihs, G.; Hilti, B. *Helv. Chim. Acta* **1981**, *64*, 2544. (f) Lin, L.-S.; Marks, T. J.; Kannewurf, C. R.; Lyding, J. W.; McClure, M. S.; Ratajack, M. T.; Whang, T.-C. *J. Chem. Soc., Chem. Commun.* **1980**, 954. (g) Wuu, Y.-M.; Peng, S.-M. *J. Inorg. Nucl. Chem.* **1980**, *42*, 839.
(5) (a) Hochgesang, P. J.; Bereman, R. D. *Inorg. Chim. Acta* **1989**, *156*, 213. (b) Hochgesang, P. J.; Bereman, R. D. *Inorg. Chim. Acta* **1988**, *149*, 69. (c) Dabrowiak, J. C.; Fisher, D. P.; McElroy, F. C.; Macero, D. J. *Inorg. Chem.* **1979**, *18*, 2304.
(6) (a) Marks, T. J. *Angew. Chem., Int. Ed. Engl.* **1990**, *29*, 857. (b) Inabe, T.; Nakamura, S.; Liang, W.-B.; Marks, T. J.; Burton, R. L.; Kannewurf, C. R.; Imaeda, K. I. *J. Am. Chem. Soc.* **1985**, *107*, 7224. (c) Schramm, C. J.; Scaringe, R. P.; Stojakovic, D. R.; Hoffman, B. M.; Ibers, J. A.; Marks, T. J. *J. Am. Chem. Soc.* **1980**, *102*, 6702.
(7) (a) Martinsen, J.; Pace, L. J.; Phillips, T. E.; Hoffman, B. M.; Ibers, J. A. *J. Am. Chem. Soc.* **1982**, *104*, 83. (b) Phillips, T. E.; Scaringe, R. P.; Hoffman, B. M.; Ibers, J. A. *J. Am. Chem. Soc.* **1980**, *102*, 3435.
(8) Ciliberto, E.; Doris, K. A.; Pietro, W. J.; Reisner, G. M.; Ellis, D. E.; Fragalà, I.; Herbstein, F. H.; Ratner, M. A.; Marks, T. J. *J. Am. Chem. Soc.* **1984**, *106*, 7748.
(9) Di Bella, S.; Casarin, M.; Fragalà, I.; Granozzi, G.; Marks, T. J. *Inorg. Chem.* **1988**, *27*, 3993 and references therein.
(10) Di Bella, S.; Fragalà, I.; Marks, T. J.; Ratner, M. A.; Cody, J. A.; Schleuter, J. A.; Schindel, J.; Kannewurf, C. R. Submitted for publication.

0020-1669/92/1331-2835$03.00/0

Table I. Ab Initio and Multipolar DV-Xα Eigenvalues and Population Analysis of the Outermost H_2TAA MO's

MO	eigenvalue,[a] eV	population,[b] %								character
		N	N′	C	C′	C″	C_{ar}[c]	H	H_{ar}[c]	
$6a_u$	(8.36) 4.91	15	20	24	2		39			π_{12}
$6b_g$	(9.78) 5.77	14	23	26	6		31			π_{11}
$5b_g$	(10.90) 6.59	6	2	1	12	20	59			π_{10}
$5a_u$	(11.52) 6.86	4	2		5	7	82			π_9
$21a_g$	(12.29) 6.07	9	61	4		4	10	11	1	n_2
$4b_g$	(12.46) 7.43	1	2	16	4	2	75			π_8
$21b_u$	(12.51) 6.12	3	67	4		6	10	10		n_1
$4a_u$	(12.80) 7.73	1	2	19	7	3	68			π_7
$3b_g$	(14.55) 8.69	10	11	1	2	10	66			π_6
$3a_u$	(15.16) 9.15	8	27	5		33	27			π_5
$20a_g$	(15.62) 9.54	2	4	9	4	6	48	10	17	σ
$2a_u$	(15.81) 9.38	17	2	4	20		57			π_4
$20b_u$	(15.87) 9.76		7	3	3	3	58	4	22	σ
$19b_u$	(16.20) 10.07	5	4	19	6	6	32	16	12	σ
$19a_g$	(16.47) 10.33	1	1	9	3	5	54	6	21	σ
$2b_g$	(16.75) 10.14	9	21	11	15	23	21			π_3
$18b_u$	(16.87) 10.44	6	2	15	4	4	38	16	15	σ
$18a_g$	(16.95) 10.51	4	3	28	3	3	33	15	11	σ
$17a_g$	(17.62) 10.79	3	6	6	16	14	31	14	10	σ
$1b_g$	(17.88) 10.88	30	2		10		58			π_2
$1a_u$	(18.20) 11.01	28	7	3	11	5	46			π_1

[a] Values of ab initio calculation are reported in parentheses. All eigenvalues have been multiplied by −1. [b] See Chart I. Contributions smaller than 1% are omitted. [c] ar = arene atoms.

Chart I

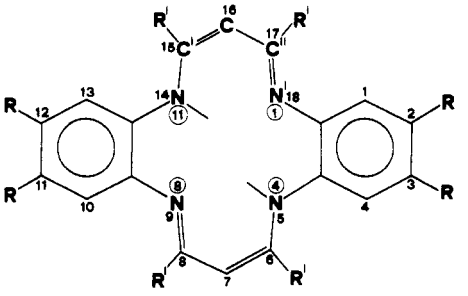

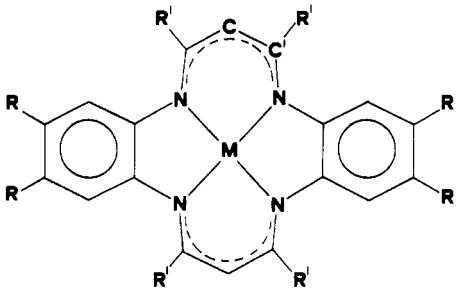

of consecutive scans was locked to the reference values of the $Ar^+ {}^2P_{3/2}$ and He $1s^{-1}$ self-ionization lines. Spectral resolution measured on the Ar $^2P_{3/2}$ lock was always better than 0.025 eV. The He II spectra were corrected only for the He IIβ "satellite" contributions (12% on reference N_2 spectrum). The procedures used for spectral deconvolution have been described elsewhere ($R \leq 0.03$).[11]

Computational Details

Pseudopotential[12] LCAO-MO-SCF calculations were carried out at the ab initio level using the PSHONDO program.[13] The specific parameters used have been reported elsewhere.[14] Gaussian basis sets[9] were contracted in a single-ζ form for nitrogen, carbon, hydrogen (4s,4p to 1s,1p contraction), and the 5p atomic orbitals (AO's) of palladium, and in a double-ζ form for the 4d and 5s AO's of palladium. The validity of the present calculational approach was previously checked on various simple square-planar Pd complexes, and it was demonstrated that the presently adopted basis sets closely reproduce results (energies and population analysis) obtained with a double-ζ quality basis set.[15] The procedures used for the evaluation of ionization energies (IE's) have been reported elsewhere.[9,16]

First-principles Hartree–Fock–Slater calculations were performed within the DV-Xα scheme.[17] Numerical AO's (through 4p on Ni, 5p on Pd, 2p on N and C, and 1s on H) were used as basis functions. In the case of Ni(TAA) and Pd(TAA), better agreement between theoretical and experimental values is found if 3s and 3p virtual N AO's are included. Because of the complexity of the present molecules, a frozen core approximation (1s, ..., 3p on Ni, 1s, ..., 3d on Pd, and 1s on N and C) has been used throughout the calculations, and these core orbitals were orthogonalized against the valence orbitals. The molecular potentials were improved by including multipolar fitting functions, which allows a very accurate description of the charge density.[18] Five radial decrees of freedom were allowed in the expansion of the density, in addition to the radial atomic density.[18] The ionization energies were evaluated within the Slater transition-state (TSIE's) formalism[19] to account for reorganization effects upon ionization.

The metrical parameters used in the calculations on H_2TAA were taken from the diffraction study of $H_2TM'TAA$[3f] (R′ = CH_3 in Chart I). This molecule has a pronounced saddle-shaped conformation because of steric interactions of the methyl groups with the arene rings.[3f] In the absence of the methyl groups, we have reasonably assumed a totally planar structure for H_2TAA (C_{2h} symmetry). In fact, optical spectra of this molecule are consistent with a planar geometry.[3c] The geometrical parameters for Ni(TAA) were taken from diffraction data[3e] assuming

(11) Casarin, M.; Ciliberto, E.; Gulino, A.; Fragalà, I. *Organometallics* **1989**, *8*, 900.
(12) (a) Pêlissier, M.; Durand, Ph. *Theor. Chim. Acta* **1980**, *55*, 43. (b) Barthelat, J. C.; Durand, Ph.; Serafini, A. *Mol. Phys.* **1977**, *33*, 159. (c) Durand, Ph.; Barthelat, J. C. *Theor. Chim. Acta* **1975**, *38*, 283.
(13) Pseudopotential adaptation (Daudey, J. P.) of HONDO 76 (Dupuis, M.; Rys, J.; King, H. F. *QCPE* **1977**, *11*, 338).
(14) (a) Molecular ab initio Calculations Using Pseudopotentials; Technical Report; Laboratoire de Physique Quantique: Toulouse, 1981. (b) Daudey, J. P.; Jeung, G.; Ruiz, M. E.; Novaro, O. *Mol. Phys.* **1982**, *46*, 67.
(15) Di Bella, S., Ph.D. Thesis, University of Catania, Italy, 1986.
(16) (a) Zagrande, G.; Granozzi, G.; Casarin, M.; Daudey, J. P.; Minniti, D. *Inorg. Chem.* **1986**, *25*, 2872. (b) Gonbeau, D.; Pfister-Guillouzo, G. *J. Electron Spectrosc. Relat. Phenom.* **1984**, *33*, 279. (c) Trinquier, G. *J. Am. Chem. Soc.* **1982**, *104*, 6969.
(17) (a) Trogler, W. C.; Ellis, D. E.; Berkowitz, J. *J. Am. Chem. Soc.* **1979**, *101*, 5896. (b) Rosen, A.; Ellis, D. E.; Adachi, H.; Averill, F. W. *J. Chem. Phys.* **1976**, *65*, 3629. (c) Averill, F. W.; Ellis, D. E. *J. Chem. Phys.* **1973**, *59*, 6412.
(18) Delley, B.; Ellis, D. E. *J. Chem. Phys.* **1982**, *76*, 1949.
(19) Slater, J. C. *Quantum Theory of Molecules and Solids. The Self-Consistent Field for Molecules and Solids*; McGraw-Hill: New York, 1974; Vol. 4.

Table II. Ab Initio and Multipolar DV-Xα Atomic Charges of H_2TAA, $(TAA)^{2-}$, and Pd(TAA)

H_2TAA[a,b]		$(TAA)^{2-}$[a,b]		PdTAA[a,b]	
				Pd	(+1.256) +0.750
N	(−0.466) −0.414				
		N	(−0.303) −0.219	N	(−0.456) −0.328
N′	(−0.357) −0.330				
C	(−0.333) −0.334	C	(−0.335) −0.340	C	(−0.350) −0.323
C′	(+0.006) −0.150				
		C′	(−0.079) −0.218	C′	(−0.045) −0.176
C″	(−0.064) −0.213				
total[c]	(−0.292) −0.188	total[c]	(−1.520) −1.220	total[c]	(−1.404) −0.918
C_{ar}[d]	(−1.448) −2.114	C_{ar}[d]	(−1.744) −2.592	C_{ar}[d]	(−1.584) −2.212
H_{ar}[e]	(+1.740) +2.302	H_{ar}[e]	(+1.264) +1.812	H_{ar}[e]	(+1.732) +2.380

[a] Values of ab initio calculation are reported in parentheses. [b] See Chart I. [c] Total charge on the 1,3-diiminopropane bridges. [d] Total charge on the arene carbon atoms. [e] Total charge on the arene hydrogen atoms.

Table III. Relevant PE Data, Computed IE's, and Assignments for the H_2TAA PE Spectrum

band label	IE, eV				rel intens[c]		
	exptl[a]	TSIE	ΔSCF	PT[b]	He I	He II	assignt[d]
a	6.68	6.87	8.02	8.15	1.00	1.00	$6a_u$
b	7.53	7.72	9.49	9.60	0.98	1.01	$6b_g$
c	8.02	8.52		10.73	1.04	1.05	$5b_g$
d	8.50	8.81		11.36	1.08	1.11	$5a_u$
		8.54	10.93	10.90			$21a_g$
e	9.08				2.03	2.10	
		8.62	10.98	10.95			$21b_u$
		9.35		12.33			$4b_g$
e′	9.50				1.96	2.04	
		9.58		12.70			$4a_u$

[a] Experimental IE's are related to the position of the Gaussian components. [b] PT = perturbative treatment. Perturbative values are obtained upon scaling repolarization contributions by a 0.75 factor (see ref 9). [c] The intensity of band a has been taken as the reference. [d] See Table I for the character of each MO.

D_{2h} symmetry. Although there are no structural data available for neutral Pd(TAA), the crystal structure of $Pd(TAA)(I_3)_{0.67}$ is known to contain planar metallomacrocyclic subunits.[4d] By extension, we have reasonably assumed a planar structure for undoped Pd(TAA). This assumption is supported by the similarity of the optical spectra of Pd(TAA) and planar[3d,e] Ni(TAA). Therefore, geometrical parameters for Pd(TAA) were adapted from the X-ray data for $Pd(TAA)(I_3)_{0.67}$[4d] and Pd(TM′TAA)[3d] (Pd–N = 1.990 Å), and also assuming D_{2h} symmetry.

Extended Hückel calculations on the model $[Ni(TAA)]_2$ cofacial dimer were performed using the EHMACC program.[20] Standard atomic parameters were used.[20] Slater-type orbitals were contracted in a single-ζ form for nitrogen, carbon, hydrogen, and the 4p and 4s AO's of nickel, and in a double-ζ form for the 3d AO's of nickel. Various conformations, including the 59° equilibrium geometry,[4d] have been examined. An interplanar distance of 3.208 Å was used as found in partially oxidized crystals.[4d]

Results and Discussion

H_2TAA Ligand. The H_2TAA ligand forms complexes with a large variety of metals.[3] It possesses a 14-atom ring containing four coordinating nitrogen atoms (Chart I) and a 24-electron ($4n$) π system.

According to both ab initio and first-principles DVM ground-state calculations (Tables I and II), the uppermost filled molecular orbitals (MO's) of the free H_2TAA ligand consist of 12 π MO's (labeled π_1–π_{12}) and two in-plane lone pairs (n_1 and n_2) localized on the nonprotonated nitrogen atoms. Results of both calculations are similar. Only minor changes of the energy sequence are noted in the case of the $21a_g$ (n_2) and $21b_u$ (n_1) MO's relative to the energetically proximate $5b_g$ and $5a_u$ orbitals (Table I). No differences are observed as far as the symmetry and nature of the HOMO is concerned since both calculations result in the same π $6a_u$ HOMO, which possesses a dominant N_{2pz} contribution (Table I).

Nodal properties and dominant populations of the uppermost eigenvectors (Table I, Figure 1) suggest some fragment-related correlations. As a matter of fact, the H_2TAA ligand can be described in terms of four main interacting fragments: (i) the two benzene rings and (ii) the two 1,3-diiminopropane bridges. The benzene π system has been widely discussed.[21] The 1,3-diimminopropane π electronic structure consists of three π MO's, one of which has dominant out-of-plane N_{2p} lone pairs. To first order, nodal properties of π_{1-4} MO's (Figure 1) suggest a correlation with the a_{2u} (D_{6h}) MO of the benzene fragment. Their energy dispersion ($(\epsilon(\pi_4) - \epsilon(\pi_1)) = 1.63$ (2.39) eV) is due (Table I) to the interactions with the out-of-plane N_{2p} lone pairs, even though the MO population as well as the energy of the π_3 MO seems to be indicative of a more profound mixing (allowed by the lower symmetry) with the more external π MO's of the diimminopropane bridges. Similarly, the π_{5-12} MO's all have nodal properties reminiscent of the benzene e_{1g} MO's (Figure 1), and their energy dispersion depends upon interactions mostly involving the more external π MO's of the 1,3-diimminopropane framework. The eight resulting MO's are spread over a large energy ($\epsilon(\pi_{12}) - \epsilon(\pi_5) = 4.24$ (6.80) eV), thus indicating a large through-bond interaction[22] between the arene moieties mediated by the 1,3-diimminopropane bridges.

Atomic p_π populations and total π overlap population values are reported in Figure 2a. Numerical analysis of p_π populations shows unitary values for arene carbon atoms, higher values ($\sim$1.64 eu) for the protonated nitrogen atoms, and alternating (1.20–0.90) values for the five-membered bridging system. The π overlap population data show a similar trend. These data are indicative of (i) a substantial delocalization within the arene π systems, (ii) a lone pair π character for the N_{2pz} orbitals on protonated nitrogen atoms, and finally (iii) a pronounced localization of π bonds in the 1–14, 5–6, and symmetry-related 7–8 and 12–13 positions of the tetraazacyclotetradecine ring.

Figure 3 shows the low IE region of the H_2TAA PE spectrum. Six resolved bands, a–e′, are present. Some small variations of the relative intensities are observed upon switching to He II

(20) Whangbo, M.-H.; Evain, M.; Hughbanks, T.; Kertesz, M.; Wijeyesekera, S.; Wilker, C.; Zheng, C.; Hoffmann, R. *QCPE* No. 571.

(21) Kimura, K., Katsumata, S., Achiba, Y., Yamazaki, T., Iwata, S., Eds. *Handbook of He I Photoelectron Spectra of Fundamental Organic Molecules*; Halsted: New York, 1981.

(22) Hoffmann, R. *Acc. Chem. Res.* **1971**, *4*, 1.

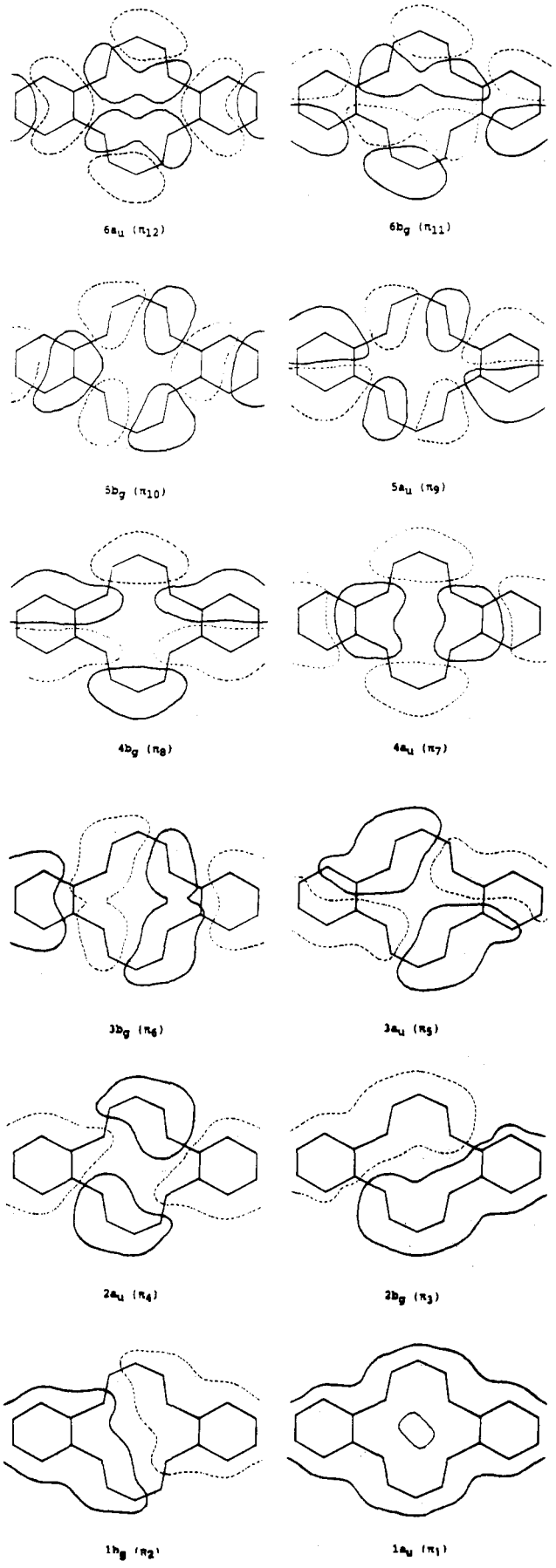

Figure 1. Multipolar Xα–DV wave function contour plots of H_2TAA for the π_{1-12} MO's 1.0 au above the H_2TAA molecular plane. The solid and dashed contours are ± 0.067 $e^{1/2}/Å^{3/2}$. The dashed lines refer to the negative part of the wave function. Plots are in the order of descending energy.

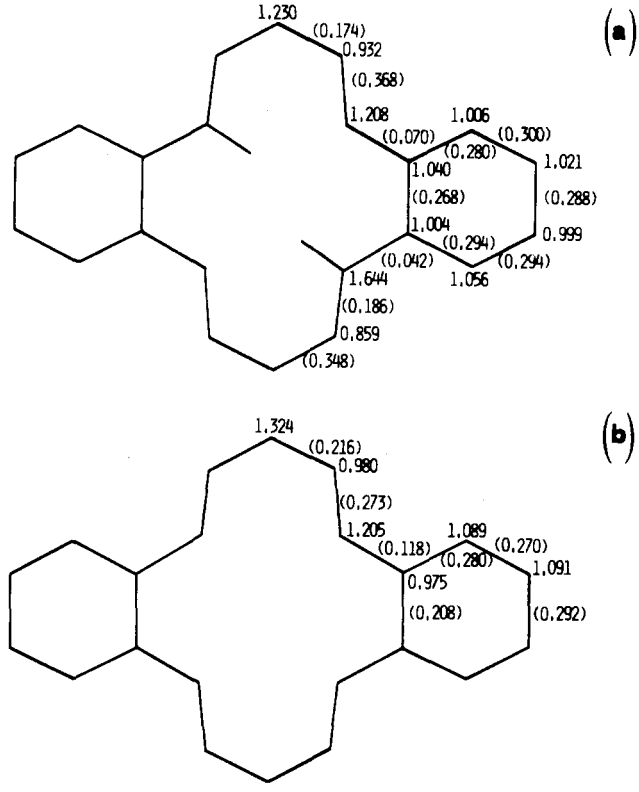

Figure 2. Atomic p_π populations and total π overlap populations (in parentheses) of (a) H_2TAA and (b) $(TAA)^{2-}$.

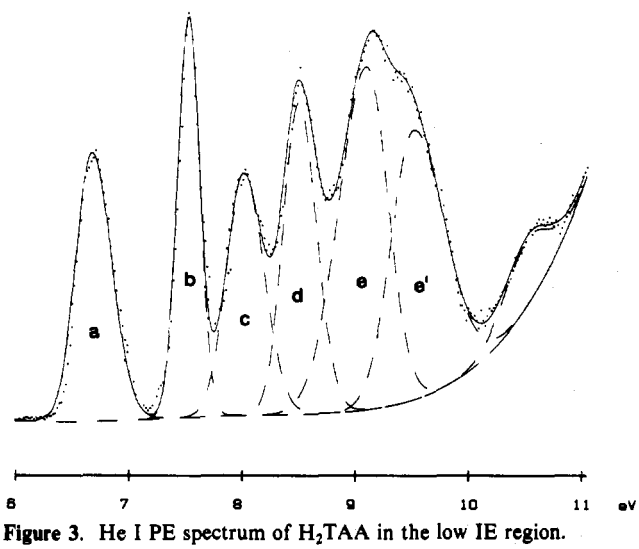

Figure 3. He I PE spectrum of H_2TAA in the low IE region.

excitation (Table III). Pertinent PE data are compiled in Table III. The experimental IE data are in good agreement with computed ΔSCF, perturbative, and TSIE values, and therefore, a general assignment of the low IE features is a straightforward matter (Table III). Worthy of note is the large experimental (2.82 eV) IE spread of ionizations associated with the π_{7-12} MO's. This value considerably exceeds the 0.95-eV e_{1g} splitting value found in *o*-phenylenediamine[23] while it lies near the 2.6-eV value found in stilbene, the conformation of which allows an easier mechanism of through-bond interaction.[24] This observation is in good accord with the aforementioned theoretical arguments. Finally, the intensity of band e, twice that found for the singly degenerate MO's (Table III), agrees well with the computed accidental degeneracy of MO's related to the N_{2p} in-the-plane lone pairs ($21a_g$ and $21b_u$ MO's). As a consequence, any through-space and/or through-bond interactions between these orbitals must be ruled

(23) Ciliberto, E.; Di Bella, S.; Fragalà, I. Work in progress.
(24) McAlduff, E. J.; Chan, T. *Can. J. Chem.* **1978**, *56*, 2714.

Table IV. Ab Initio and Multipolar DV-Xα Eigenvalues and Population Analysis of the Outermost $(TAA)^{2-}$ Dianion MO's

MO	eigenvalue,[a] eV	population,[b] %						character
		N	C	C′	C_{ar}[c]	H	H_{ar}[c]	
$4b_{1u}$	(0.79) 2.79	40	25		35			π_{12}
$3b_{3g}$	(−0.89) 1.84	41	31		28			π_{11}
$9b_{1g}$	(−2.49) 3.45	82	3	3	6	5	1	n_-
$3b_{2g}$	(−2.82) 0.52	14		52	34			π_{10}
$10b_{2u}$	(−3.37) 2.75	81	3	5	4	6	1	n_-
$11b_{3u}$	(−3.38) 2.76	77	2	2	12	6	1	n_+
$2a_u$	(−4.18) −0.06	19		31	50			π_9
$12a_g$	(−4.37) 1.85	77	3	4	11	5		n_+
$2b_{3g}$	(−5.22) −0.78		10	9	81			π_8
$3b_{1u}$	(−5.31) −0.86		19	19	62			π_7
$1a_u$	(−6.42) −1.47	27		17	56			π_5
$2b_{2g}$	(−6.84) −1.64	19		8	73			π_6
$2b_{1u}$	(−7.78) −2.09	16	13	35	36			π_4
$1b_{3g}$	(−7.85) −2.16	23	16	48	13			π_3
$11a_g$	(−7.90) −3.02	12	25	16	22	17	8	σ
$9b_{2u}$	(−8.04) −3.13	14	32	17	13	22	2	σ
$10b_{3u}$	(−8.86) −3.58	5		4	64		27	σ
$10a_g$	(−9.44) −3.92	2	14	4	50	7	23	σ
$8b_{1g}$	(−9.50) −4.00	7	1	11	56	4	21	σ
$1b_{2g}$	(−9.80) −3.62	5		1	94			π_2
$1b_{1u}$	(−9.89) −3.66	7		3	90			π_1

[a] Values of ab initio calculation are reported in parentheses. [b] See Chart I. Contributions smaller than 1% are omitted. [c] ar = arene atoms.

Table V. Multipolar DV-Xα Eigenvalues[a] and Population Analysis of the Outermost Pd(TAA) MO's

MO	eigenvalue,[c] eV	population,[b] %									overlap populn Pd-N	dominant character
		Pd			N	C	C′	C_{ar}[d]	H	H_{ar}[d]		
		4d	5s	5p								
$4b_{1u}$	5.09 (8.28)				35	25		40			0.000	π_{12}
$4b_{3g}$	5.57 (9.37)	19			32	24		25			−0.055	π_{11}, d_{yz}
$14a_g$	6.13 (11.49)	67			28	1	1	2	1		−0.022	d_{z^2}, n_+
$4b_{2g}$	6.64 (10.52)	12			10		43	35			−0.026	π_{10}, d_{xz}
$2a_u$	7.11 (11.40)				5		11	84			0.000	π_9
$3b_{2g}$	7.31 (12.95)	61					1	38			0.000	d_{xz}
$3b_{3g}$	7.44 (12.23)	54				1	2	43			0.000	d_{yz}
$2b_{3g}$	7.63 (13.72)	18			3	22	14	43			0.009	π_8, d_{yz}
$3b_{1u}$	7.83 (12.66)				3	18	13	66			0.000	π_7
$11b_{3u}$	8.00 (13.39)			2	63	3	8	13	10	1	0.094	n_+
$10b_{2u}$	8.01 (13.40)			1	66	5	7	11	9	1	0.071	n_-
$13a_g$	8.05 (14.72)	85			6	1	3	4	1		−0.031	$d_{x^2-y^2}$
$2b_{2g}$	9.11 (15.15)	13			14		6	67			0.022	π_6, d_{xz}
$2b_{1u}$	9.38 (15.39)				6	10	26	58			0.000	π_4
$1a_u$	9.44 (15.25)				57		26	17			0.000	π_5
$12a_g$	9.76 (15.60)	11	2		12	7	5	40	9	14	0.050	σ, $d_{x^2-y^2}$, d_{z^2}
$9b_{1g}$	10.08 (15.31)	15			8	3	5	48	3	18	0.018	σ, d_{xy}
$9b_{2u}$	10.18 (15.98)				10	25	11	27	17	10	0.000	σ
$10b_{3u}$	10.26 (15.86)				5	1	1	63		30	0.000	σ
$11a_g$	10.37 (16.54)	10			33	30	8	9	9	1	0.073	n_+, d_{z^2}
$1b_{3g}$	10.46 (16.96)	9			40	8	38	5			0.020	π_3, d_{yz}
$8b_{1g}$	10.64 (16.60)	13			6	4	23	33	10	11	0.029	σ, d_{xy}
$8b_{2u}$	10.65 (16.82)				5	22	3	41	9	20	0.000	σ
$10a_g$	10.81 (16.92)	4	1		13	13	5	35	14	15	0.009	σ, d_{z^2}, $d_{x^2-y^2}$
$1b_{2g}$	11.14 (17.78)	6			30		6	58			0.016	π_2, d_{xz}
$1b_{1u}$	11.19 (16.96)				30	2	16	52			0.000	π_1

[a] 3s and 3p N AO's are included. [b] See Chart I. Contributions smaller than 1% are omitted. [c] Eigenvalues of ab initio calculation are reported in parentheses. All eigenvalues have been multiplied by −1. [d] ar = arene atoms.

out.

Metal Complexes. An accurate description of perturbations induced in the ligand electronic system due to complex formation requires a full understanding of effects due to (i) deprotonation and related charge redistribution and (ii) interactions with relevant metal orbitals.

Deprotonation of H_2TAA causes a large electronic charge redistribution due mainly to localization of the negative charge on the 1,3-diimminopropane bridges (Table II). Major changes are observed in the MO populations (Tables I and IV) of the $12a_g$ (n_+), $11b_{3u}$ (n_+) and $10b_{2u}$ (n_-), $9b_{1g}$ (n_-) MO's, all of which represent in-the-plane symmetry combinations of nitrogen lone pairs. Furthermore, the p_π population and π overlap values are indicative of more pronounced π charge delocalization than in H_2TAA (Figure 2b).

Eigenvalues and population analyses of the ground-state multipolar DV-Xα and ab initio calculations on Pd(TAA) are reported in Table V. The bonding of the metal atom to the $(TAA)^{2-}$ dianion ligand results in severe perturbations of the ligand σ and π electronic structure because of a large orbital admixture with the metal d subshells (Table V). In particular, the metal d_{z^2} orbital strongly interacts with the $(TAA)^{2-}$ $12a_g$ (n_+) MO to form the bonding $11a_g$ and the antibonding $14a_g$ MO's (Table V). Moreover, the virtual d_{xy} metal orbital mixes with and in turn mixes the $9b_{1g}$ (n_-) and $8b_{1g}$ (σ) MO's of the dianion ligand. Finally, the metal 4d orbitals of π symmetry (d_{xz}, d_{yz}), intermediate in energy between the π_{1-12}-related ligand MO's, are admixed with almost all ligand MO's of appropriate symmetry (Table V).

The $4b_{1u}$ HOMO is π in character and is delocalized over the entire molecule (Figure 4a), reminiscent of the a_{1u} HOMO in

Table VI. Photoelectron Spectroscopic Data and Assignments for Pd(TAA) and Pd(TMTAA)

band label	Pd(TAA) IE,[a] eV	Pd(TAA) rel intens[b] He I	Pd(TAA) rel intens[b] He II	Pd(TMTAA) IE,[a] eV	Pd(TMTAA) rel intens[b] He I	Pd(TMTAA) rel intens[b] He II	IE[c]	C_{ar},[d] %	assignt[e]
a	6.42	1.00	1.00	6.30	1.00	1.00	0.12	40 (13)	$4b_{1u}$
b	6.90	1.12	1.08	6.80	1.19	1.16	0.10	25 (8)	$4b_{3g}$
c	7.77	0.94	0.80	7.60	0.99	0.95	0.17	35 (14)	$4b_{2g}$
d′				8.19	1.75 [0.85	0.75	0.16	84 (13)	$2a_u$
d	8.35	1.80	2.16	8.37	0.90]	1.37	−0.02	2 (0)	$14a_g$
e	8.85	1.81	1.96	8.76	1.75	1.93	0.09	[43 (5) [43 (4)	$3b_{3g}$ $2b_{3g}$
e′				8.97	1.94 [0.90	0.88	0.30	66 (41)	$3b_{1u}$
f	9.27	1.80	2.01	9.25	1.04]	1.31	0.02	38 (14)	$3b_{2g}$
g	9.57	1.09	1.45	9.60	1.01	1.35	−0.03	4 (0)	$13a_g$
h	9.98	2.19	2.05	10.00	2.14	2.04	−0.02	[13 (2) [11 (1)	$11b_{3u}$ $10b_{2u}$

[a] Experimental IE's are related to the position of Gaussian components. [b] The intensity of band a has been taken as reference. [c] Experimental IE shift passing from Pd(TAA) to Pd(TMTAA). [d] Percentage on the arene ring carbons (from Table V). Values in parentheses refer to the percentage on the arene ring carbons α to the methyl groups. [e] See Table V for the character of each MO.

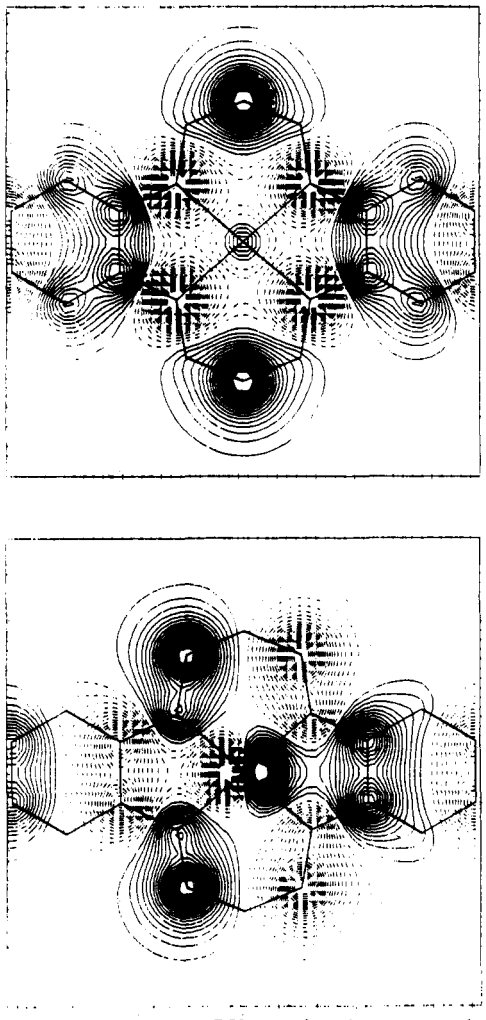

Figure 4. Multipolar Xα–DV wave function contour plots of Pd(TAA) for the (a) $4b_{1u}$ and (b) $4b_{2g}$ MO's 1.0 au above the Pd(TAA) molecular plane. The interval between successive contours is 0.034 $e^{1/2}/Å^{3/2}$. The dashed lines refer to the negative part of the wave function.

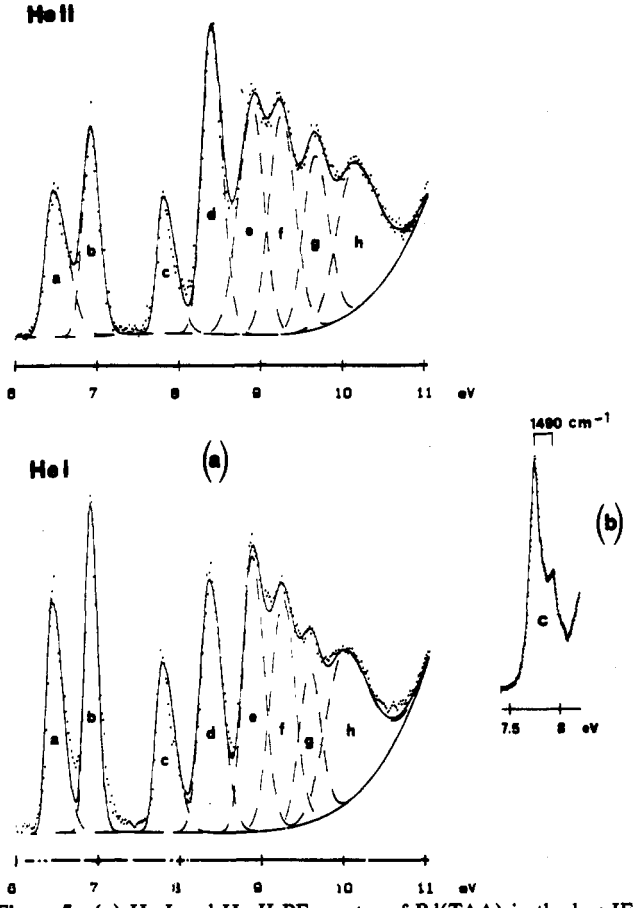

Figure 5. (a) He I and He II PE spectra of Pd(TAA) in the low IE region: experimental spectrum (dotted lines); Gaussian components (dashed lines); convolution of Gaussian components (solid line). (b) High-resolution expanded scale of band c.

porphyrin and phthalocyanine complexes.[8,25] However, the $4b_{1u}$ HOMO shows quite different nodal properties. Variations of atomic charge values (Table II) provide indications of the charge redistribution occurring upon the Pd^{2+} bonding. In particular, an increase of the negative charge on the donor nitrogen atoms and a parallel charge decrease on the arene rings are noted.

The He I and He II PE spectra of Pd(TAA) and Pd(TMTAA) (Figures 5 and 6) are similar, exhibiting eight main structural features (a–h) in the region below 11 eV. In the spectrum of Pd(TMTAA), however, the band d is clearly resolved into two components (d and d′) while a shoulder (e′) is associated with band e. Furthermore, a generally small upward shift in IE's (~0.15 eV) is observed on passing from Pd(TAA) to Pd(TMTAA) (Table VI). Variations of relative intensities (Table VI) are observed upon switching to He II radiation, and in both cases, bands d–g increase moderately relative to band a. Finally, fine structure is associated with band c in the spectrum of Pd(TAA) (Figure 5b).

The experimental IE data compare well with the Xα TSIE, ab initio ΔSCF, and perturbative values (Table VII). TSIE's provide, however, a better fitting in terms of both absolute values and IE grouping (Table VII). Thus, Pd(TAA) bands d–g, more intense

(25) Kutzler, F. W.; Ellis, D. E. *J. Chem. Phys.* **1986**, *84*, 1033.

Table VII. Comparison of Computed and Experimental IE's for Pd(TAA) and Ni(TAA)

Pd(TAA)					Ni(TAA)		
	computed IE, eV					computed	
MO	ΔSCF	PT[b]	TSIE	exptl IE,[a] eV	MO	TSIE	exptl IE,[a] eV
$4b_{1u}$	7.85	8.05	7.02	6.42 (a)	$4b_{1u}$	7.27	6.59 (a)
$4b_{3g}$	8.94	9.10	7.58	6.90 (b)	$4b_{3g}$	7.34	6.87 (b)
$4b_{2g}$	10.20	10.35	8.57	7.77 (c)	$4b_{2g}$	9.25	7.73 (c)
$2a_u$	11.06	11.24	9.06	8.35 (d)	$3b_{2g}$	8.71	8.30 (d)
$14a_g$	9.30	9.28	9.39		$14a_g$	8.75	
$3b_{3g}$		12.09	9.48	8.85 (e)	$2a_u$	8.97	8.53 (d')
$2b_{3g}$	11.17	11.16	9.60		$3b_{3g}$	9.08	8.77 (e)
$3b_{1u}$		12.56	9.68	9.27 (f)	$2b_{3g}$	9.48	9.11 (f)
$3b_{2g}$		11.45	9.87		$3b_{1u}$	9.69	9.27 (g)
$13a_g$		12.80	11.24	9.57 (g)	$13a_g$	9.89	
$11b_{3u}$		12.51	10.21	9.98 (h)	$11b_{3u}$	10.57	10.02 (h)
$10b_{2u}$		12.43	10.25		$10b_{2u}$	10.84	

[a] Band labels are given in parentheses. [b] PT = perturbative treatment. Perturbative values are obtained upon scaling repolarization contributions by a 0.75 factor (see ref 9).

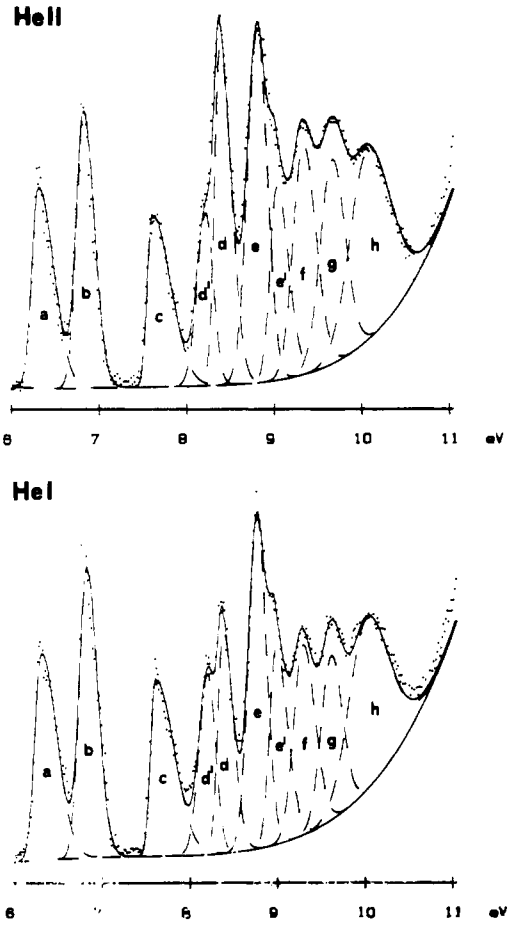

Figure 6. He I and He II PE spectra of Pd(TMTAA) in the low IE region: experimental spectrum (dashed lines); Gaussian components (dashed lines); convolution of Gaussian components (solid line).

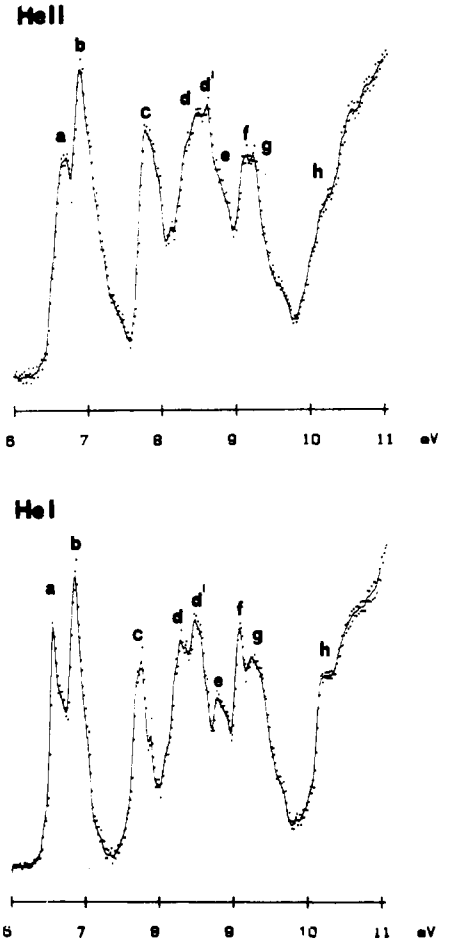

Figure 7. He I and He II PE spectra of Ni(TAA) in the low IE region.

in the He II spectrum, are assigned to ionizations from the $14a_g$ and $2a_u$, $3b_{3g}$ and $2b_{3g}$, $3b_{2g}$, and $13a_g$ MO's, respectively, in accordance with their dominant metal d character[9] (Table V). The remaining bands (a–c, and h) are associated with ionizations of ligand-based MO's. This general assignment is consistent with some additional, experimental evidence. In particular bands a–c find close counterparts in the spectrum of the free H_2TAA ligand (Figures 3 and 5 and Tables III and VI), and the remarkable 0.63 eV lower IE shift associated with band b is in accordance with the Pd–N antibonding nature of the corresponding $4b_{3g}$ MO (Table V). Moreover, IE's associated with bands d and f suffer a differential lower IE shift relative to the rest of the bands on passing from Pd(TAA) to Pd(TMTAA), and this effect nicely reproduces the larger amplitude of corresponding MO's (Table VI) on the arene ring carbons α to the methyl groups.[26,27] Finally, the 1490 ± 100 cm^{-1} progression associated with band c in the PE spectrum of Pd(TAA) (Figure 5b) agrees well with the IR-active transition assigned to a macrocyclic skeletal deformation at 1581 cm^{-1}.[3c] This observation strongly supports a coexcitation of skeletal vibration modes upon ionization from the $4b_{2g}$ MO. Furthermore, the smaller vibrational interval (with respect to that found in the IR spectrum) measured in the PE spectrum underscores the C–N and C–C bonding nature of $4b_{2g}$ MO (Figure 4b).

The PE spectrum of Ni(TAA) (Figure 7) is closely analogous with that of the Pd analogue. Full coincidence of the relevant

(26) Libit, L.; Hoffmann, R. *J. Am. Chem. Soc.* **1974**, *96*, 1370.
(27) Calabro, D. C.; Hubbard, J. L.; Blevins, C. H.; Campbell, A. C.; Lichtenberger, D. L. *J. Am. Chem. Soc.* **1981**, *103*, 6839.

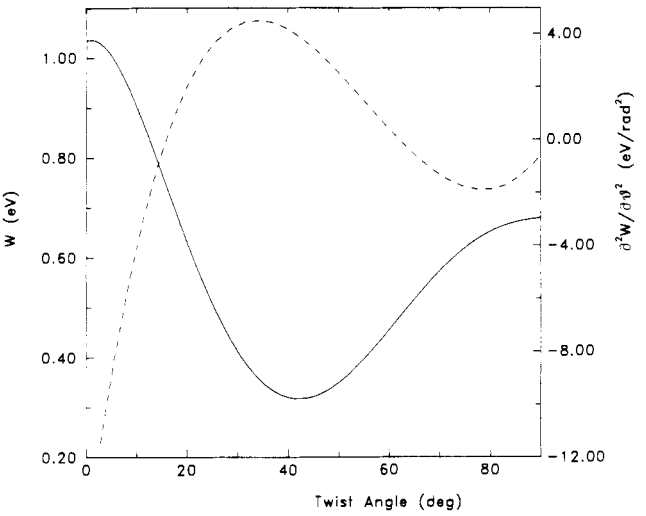

Figure 8. Variation of valence bandwidth (W, solid line) and of $\delta^2W/\delta\vartheta^2$ (dashed lines) with staggering twist angle in the cofacial $[Ni(TAA)]_2$ dimer (interplanar distance 3.208 Å). An angle of 0° corresponds to a completely eclipsed conformation.

PE data (Table VII) is noted as far as bands a–c are concerned, while the shape of the d–h envelope is somewhat different. TSIE's (Table VII) provide an indication of the same topmost 12 ionizations as found in Pd(TAA) even though minor differences in their sequence are observed (Table VII). Therefore, while the assignment of bands a–c can be conclusive and analogous to that proposed for Pd(TAA), there remain ambiguities concerning a detailed assignment of bands d–h. This is because the He II spectrum (Figure 7) does not provide any relevant details and there is no further additional experimental evidence as found for Pd(TAA) (vide supra).

Charge-Transport Properties of TAA-Based Polymers

It has been demonstrated that the condensed-phase electrical, optical, and magnetic properties of partially oxidized molecular conductors depend mostly upon favorable overlap involving frontier orbitals of the stacked units modulated by the spatial orientation and chain structure existing in the crystals.[2] Furthermore, since these 1-D systems have quite narrow bandwidths, the coupling of the conduction electrons to intramolecular phonons and/or librations can contribute to the resistivity along the chain.[28]

In all of the present TAA-based cases, the HOMO consists of a π orbital, of b_{1u} symmetry, fully localized on the macrocyclic ligand. The lack of any metal d admixture into this MO is in excellent agreement with the experimental observation that electrical conductivities of partially oxidized TAA complexes do not depend greatly on the nature of the metal ion.[4] Furthermore, it is worth noting that the $4b_{1u}$ HOMO contour plot (Figure 4a) shows a pattern indicative of a wave function whose sign does not change in a 2.5-Å region around the metal.

It is well known that the dimer model approximation[28b] allows, within a simple tight-binding band picture,[2] extrapolation of the HOMO–HOMO energy spitting to the bandwidth in the infinite 1-D stack. Crystal structure data on relevant 1-D TAA complexes show that the macrocyclic subunits are stacked along the c axis of the crystal and staggered by 59° in $Ni(TAA)(I_3)_{0.67}$,[4d] and by 54° in $Pd(TAA)(I_3)_{0.67}$.[4d] EH calculations on the model cofacial dimer $[Ni(TAA)]_2$ demonstrate that the HOMO–HOMO interaction, and hence the tight-binding bandwidth ($W = 4t$) in the corresponding infinite stack, reaches a *minimum* for all the conformations near the staggering angle found in the crystals (Figure 8). In interesting contrast, the ligand-centered HOMO wave function has been found to have a_{1u} symmetry in phthalocyanine complexes, thus having eight nodal points around the z (stacking) axis.[8] In this case, the bandwidth possesses a *maximum* value near the equilibrium staggering angle (~40°).[28b] This factor no doubt contributes to the higher (than in TAA) stacking axis conductivity[6] of the partially oxidized M(Pc) materials. A straightforward consequence of this observation is that twisting motions (librations) should have different effects upon the bandwidth values (hence the temperature dependence of charge transport) as far as the two classes of stacked materials are concerned.

Evaluation of the libron-coupling-related quantity[28a] $\delta^2W/\delta\vartheta_o^2$ for $Ni(TAA)(I_3)_{0.67}$ (Figure 8) leads to a 0.60 eV/rad^2 value which can be compared with a 5.45 eV/rad^2 value calculated for $Ni(Pc)(I_3)_{0.33}$ in the staggered ($\vartheta_o = 39.5°$) geometry.[28a] Therefore, within the simple phonon-scattering model already adopted to describe the conductivity mechanism in phthalocyanine-based "molecular metals",[28a] the present results argue that libron-scattering processes should scarcely affect resistivity values of TAA-based materials.

Acknowledgment. E.C., A.G., and I.F. gratefully thank the Consiglio Nazionale delle Ricerche (CNR, Rome, Progetto Finalizzato Materiali Avanzati) for financial support. This research has also been supported in part by the NATO Research Grants Program (Grant 068/84 to I.F. and T.J.M.) and by the Materials Research Center of Northwestern University (NSF Grant DMR 8821571 to T.J.M.).

Registry No. Pd(TAA), 68833-20-5; Pd(TMTAA), 76565-81-6; Ni(TAA), 39251-81-5; H_2TAA, 900-17-4.

(28) (a) Hale, P. D.; Ratner, M. *J. Chem. Phys.* **1985**, *83*, 5277. (b) Pietro, W. J.; Marks, T. J.; Ratner, M. A. *J. Am. Chem. Soc.* **1985**, *107*, 5387. (c) Weger, M.; Kaveh, M.; Gutfreund, H. *Solid State Commun.* **1981**, *37*, 421. (d) Gutfreund, H.; Hatstein, Weger, M. *Solid State Commun.* **1980**, *36*, 647. (e) Conwell, E. M. *Phys. Rev. B* **1980**, 1761.